JOURNAL OF MATERIALS SCIENCE **34** (1999) 3695–3707

Simulation of craze failure in a glassy polymer: rate dependent drawing and rate dependent failure models

Y. SHA, C. Y. HUI*
Department of Theoretical and Applied Mechanics, Cornell University, Ithaca, NY 14853
E-mail: yan_sha@ccm.ch.intel.com

E. J. KRAMER‡
Department of materials Science and Engineering and the Materials Science Center, Cornell University, Ithaca, NY 14853

The failure of a craze ahead of a crack growing under steady state conditions in a glassy polymer is investigated by modeling the craze microstructure using a highly anisotropic network of springs. A rate dependent drawing law is used to determine the shape of the craze-bulk interface. Approximate analytical results are developed to link the normal stress on the craze-bulk interface, the thickness of the craze and the far field stress intensity factor to the crack propagating velocity, through the craze failure criterion and the craze microstructural parameters. The accuracy of the analytical results is examined using a detailed numerical simulation. Our analysis shows that the rate independent craze failure criterion, which assumes the failure stress for fibrils ahead of the crack tip to be a material constant independent of the crack growth rate, leads to predictions of the dependence of the craze thickness and the fracture toughness on crack growth rate that are contrary to what is found experimentally. Rate dependent craze failure criteria are then proposed. Specifically, we study a case where the crack tip fibril breaks down by rate dependent chain scission and a case where the crack tip fibril fails by rate dependent chain disentanglement. For the rate dependent chain scission criterion, the results given by the rate independent constant failure stress criterion are retrieved in the limit of low crack propagation velocity. Also, there exists a critical stress intensity factor below which steady state crack propagation is impossible, i.e., crack growth becomes unstable.

1. Introduction

The fracture of glassy polymers is linked to the stress-induced growth and breakdown of crazes, which are planar crack-like defects. But unlike cracks, the two surfaces of crazes are bridged by many fine fibrils which give crazes some load bearing capacity. It is well known that the craze grows in length by the Taylor meniscus instability [1, 2] and grows in width by surface drawing [1], in which the polymer chains are drawn from strain-softened bulk into the fibrils. The volume fraction of the crazed material is approximately uniform along the craze [1]. Experiments indicate that the drawing stress σ_d along the craze-bulk interface is also approximately uniform, except near the crack tip and the craze tip [1]. This approximate uniform traction along the craze-bulk interface motivates the use of the Dugdale model [3] to calculate the craze opening displacement which is used as the failure criterion for the craze, i.e., the craze will fail when the crack tip opening displacement reaches a critical value, δ_c. Within the framework of the Dugdale model, the critical crack tip opening displacement δ_c cannot be determined and is treated as a fitting parameter.

Consistent with the Dugdale model, the fibrils inside the craze were historically modeled as parallel cylinders perpendicular to the craze surface. This assumption of parallel fibrils and the constant drawing stress (Dugdale model) implies that there is no lateral load transfer between individual fibrils so that the force on every fibril is identical, i.e., there is no stress concentration inside the craze so that the craze can draw indefinitely. This means that the critical crack tip opening displacement $\delta_c = \infty$. This apparent paradox was resolved by Brown [5], who proposed a mechanism of craze failure based on the observation from transmission electron micrographs (TEM) of crazes which

* Authors to whom all correspondence should be addressed.
‡ *Present address*: Department of Materials, UCSB, Santa Barbara, CA 93106.

reveal the existence of short fibrils running between the main tensile fibrils [4]. Brown [5] pointed out that the existence of these "cross-tie" fibrils has a profound effect on the failure mechanism of the craze. The cross-tie fibrils can transfer load between main fibrils thus allowing the force in the first fibril ahead of the crack tip to reach the breaking force.

One of the difficulties in modeling the process of craze breakdown is the specification of the boundary conditions along the craze-bulk interface, since the location and shape of the craze-bulk interface are determined by the drawing law of the craze fibrils, mass conservation of the craze material, the elastic response of the bulk material outside the craze and the continuity of traction and displacement across the craze-bulk interface. The difficulty of this fully coupled problem is avoided by Brown [5] who modeled the crack tip craze material as an infinite strip of highly anisotropic elastic continuum with elastic moduli C_{ij}. Fig. 1 shows the relative scale of the problem. The length of the craze L is much smaller than the crack length a, which in turn is much smaller than w, the width of the specimen. The thickness of the craze at the crack tip $2h_c$ is much smaller than L but is substantially larger than the fibril spacing. Thus the geometry in Fig. 1b is approximated by an infinite strip with thickness h_c (Fig. 1c). Due to symmetry, only half the craze needs to be considered. The effect of crack tip loading is simulated by applying a uniform displacement on the strip boundary, which is determined by the condition that the stress far away from the crack tip is uniaxial and is equal to the drawing stress σ_d. Specifically, a uniform displacement $\Delta = (\sigma_d/C_{22})h_c$ is applied on the craze boundary, where C_{22} is the tensile modulus of the craze in the direction of the main fibrils. h_c is the half thickness of the strip and is related to the critical crack tip opening displacement δ_c by:

$$\delta_c = 2h_c(1 - v_f) \tag{1}$$

where v_f is the volume fraction of the fibrillated material and is found to be a material constant [1].

The strip model predicts that the tensile stress ahead of the crack tip has the classical inverse square root singularity that scales with $\sqrt{h_c\alpha_0}$, where $\alpha_0^2 = C_{66}/C_{22}$ and C_{66} is the in-plane shear modulus of the crazed material. The craze is assumed to fail when the average tensile stress in the first fibril ahead of the crack tip reaches the critical value of σ_f where σ_f is assumed to be a material constant and independent of the crack growth rate. Using this failure criterion, and the crack tip singular field, Brown showed that the critical crack tip opening displacement δ_c is

$$\delta_c = \frac{\pi D_0}{\alpha_0}(1 - v_f)\left(\frac{\sigma_f}{\sigma_d}\right)^2 \tag{2}$$

where D_0 is on the order of a fibril spacing. The key idea of Brown's strip model is to show that the failure of craze, e.g., δ_c cannot be predicted using a line zone with zero thickness as in the Dugdale model. Instead, the microstructural details of the craze as well as its thickness have to be included in the analysis.

Several improvements on Brown's model have been suggested. (1) Hui *et al.* [6] extended Brown's model using anisotropic elasticity to determine the full continuum stress field inside the craze. (2) Sha *et al.* [7] replaced the anisotropic continuum with a spring network model to investigate the effects of craze microstructure. (3) Sha *et al.* [8] replaced Brown's assumption of a uniform displaced strip with a more realistic stress distribution on the craze boundary derived from an assumed rate independent drawing law.

The aforementioned calculations [5–8] neglect the fact that crack growth in polymer glasses due to craze breakdown is a rate dependent process which was demonstrated experimentally by Döll [9] and Dai *et al.* [10]. Previous analysis by Kramer and Hart [11] and Knauss *et al.* [12] included rate dependence in their crack growth model but still treated the craze (or the fracture process zone in Knauss's model) as a line zone of zero thickness. The two dimensional nature of load transfer between the fibrils inside the craze, which is shown to be critical in the understanding of the craze failure process, is not considered.

In this paper, the shape of a craze ahead of a steadily growing crack is predicted using a rate dependent drawing law, i.e.,

$$\dot{h} = \alpha\left(\frac{\sigma_n}{\sigma_0}\right)^n \tag{3}$$

where σ_n is the normal stress on the craze bulk interface at a fixed material point. Here α is a material constant with dimensions of velocity, σ_0 is a material parameter which is often taken as the nominal drawing stress, n is

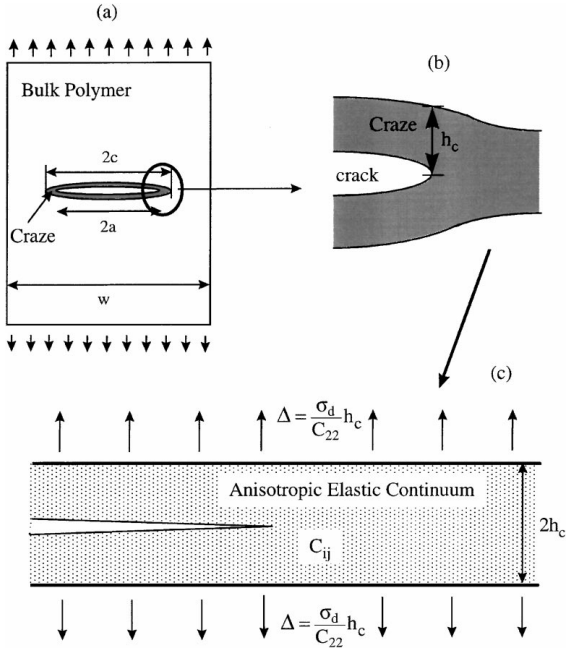

Figure 1 Figure 1 shows the relative scale of the problem. The length of the craze L is much smaller than the crack length a, which in turn is much smaller than w. The thickness of the craze at the crack tip $2h_c$ is much smaller than L but is substantially larger than the fibril spacing. Thus the geometry in Fig. 1b is approximated by an infinite strip with thickness h_c (Fig. 1c).

a material parameter and is typically on the order of 10 or larger [13]. The craze is no longer assumed to have zero thickness or to be a strip with uniform thickness as in previous studies [5–10]. It has finite thickness and the craze thickness profile, $h(x)$, is calculated through the mass conservation of the crazed material and the stress and displacement continuity across the craze-bulk interface.

The aim of this paper is to study the dependence of the crack growth rate on the applied stress intensity factor, the drawing law, the craze microstructural parameters and the possible failure criteria of the craze. Analytical approximate solutions are developed to study the failure of the craze. The effect of rate dependence of the problem comes in through the drawing law, the crack growth rate and the fact that the failure process may be rate dependent. As in previous work [5–8], we first consider the rate independent failure criterion and we demonstrate that the rate independent craze failure criterion leads to predictions which are contrary to the experimental observations. This motivates us to include the rate effects in the craze failure model. We then propose two rate dependent craze failure criterion, i.e., (1) rate dependent chain scission and (2) rate dependent chain disentanglement. Analyses are conducted for the rate dependent failure criterion and good agreement is found between the simulation and the experiments.

2. Problem formulation

2.1. Geometry

The geometry is shown in Fig. 2. As in all previous calculations, we assumed small scale yielding (SSY) condition [14–16], since the length of the craze is small compared to the length of the crack and the specimen dimensions so that the far field applied elastic stress intensity factor K_A controls the growth of the craze. Steady state crack propagation is assumed. A moving coordinate system (x, y) is attached to the crack tip (see Fig. 2) which moves along the positive x direction with a constant velocity $\dot{a}$, thus:

$$x = X - \dot{a}t \tag{4}$$

where the Cartesian coordinate system (X, Y) are fixed at one material point. The craze has its tip at $x = L$. The far field loading is Mode I and is given by [16]:

$$\sigma_{ij}(r \to \infty, \theta) = \frac{K_A}{\sqrt{2\pi r}}\sigma_{ij}(\theta)$$

where $\sigma_{ij}(\theta)$ are universal functions describing the angular variation of the in-plane stress components [16]. Note that the craze is no longer assumed to have zero thickness as in [11] and [12]. The unknown shape of the craze-bulk interface is denoted by $y = h(x)$ and will be obtained by solving a fully coupled interior-exterior problem as we will show next.

2.2. Elastic field outside the craze

The craze is assumed to have an unknown shape of $h(x)$ with unknown traction $-\sigma_n(x)$ acting on its surface. The traction $\sigma_n(x)$ and the craze shape $h(x)$ are determined by the continuity of traction and displacement along the craze-bulk interface, the drawing law and the mass conservation condition. From the continuity of displacement across the craze-bulk interface and mass conservation, the displacement of the crack face as seen by the outer elastic field, $v_c(x)$ can be shown as [1, 8]:

$$v_c(x) = h(x)(1 - v_f) \tag{5}$$

where the small elastic stretch of the craze material is neglected and v_f is the volume fraction of the fibrillated material. The factor $(1 - v_f)$ results from mass conservation, i.e., the original height of the uncrazed material must be subtracted from $h(x)$ to obtain the displacement of the glassy material above the interface. A detailed discussion of Equation 5 can be found elsewhere [1, 8].

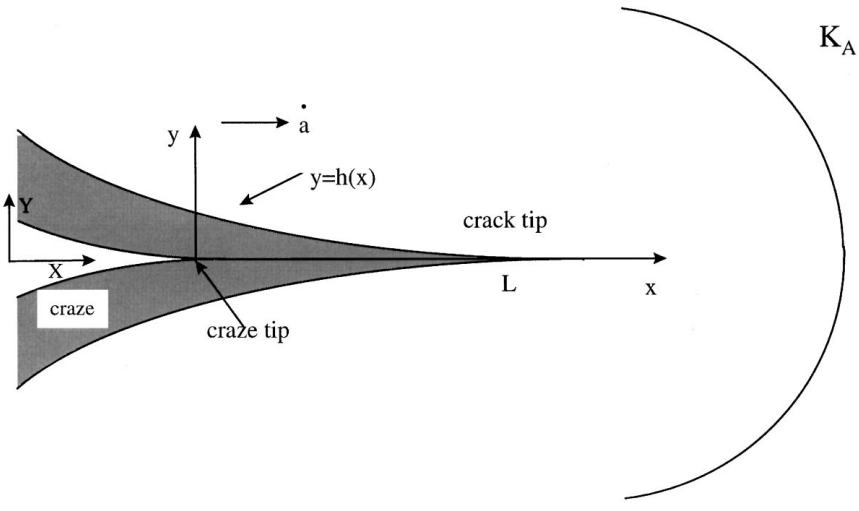

Figure 2 Small scale yielding condition: the craze of length L is assumed to be small compared with the crack length a so that the crack can be modeled as semi-infinite. The loading is simulated by the K_A field applied at ∞. (X, Y) is a Cartesian. coordinate fixed at a material point and (x, y) is the moving system with its origin fixed at the crack tip.

The glass outside the craze is modeled as a linear elastic, isotropic continuum with Young's modulus E and Poisson's ratio ν. For a given far field loading K_A, $v_c(x)$ can be expressed in terms of K_A and the normal traction $-\sigma_n(x)$ on the crack faces [17], i.e.,

$$v_c(x) = \frac{2(1-\nu^2)}{\pi E}\left(2\pi K_A\sqrt{\frac{L-x}{2\pi}} - \int_{-\infty}^{L}\sigma_n(s)\log\left|\frac{\sqrt{L-x}+\sqrt{L-s}}{\sqrt{L-x}-\sqrt{L-s}}\right|ds\right) \tag{6a}$$

The location of the craze tip, $x = L$, is determined by enforcing the condition of bounded stresses at the craze tip, which gives [17]

$$K_A = \int_{-\infty}^{L}\frac{\sqrt{2}\sigma_n(s)}{\sqrt{\pi(L-s)}}ds \tag{6b}$$

Note that both $\sigma_n(x)$ and $v_c(x)$ (i.e., $h(x)$) are unknown and their values depend on the crack growth rate and the drawing law.

2.3. Drawing law

As mentioned earlier, the craze shape $h(x)$ is determined by the drawing law which specifies how fibrils are drawn from the craze-bulk interface. In this work we consider a power law drawing law (Equation 3), i.e.,

$$\dot{h}(X,t) = \alpha\left(\frac{\sigma_n(X,t)}{\sigma_0}\right)^n$$

Under the steady state condition (Equation 4) $h(X,t) = h(x)$, the material derivative $\dot{h}(X,t)$ is

$$\left(\frac{\sigma_n(x)}{\sigma_0}\right)^n = -\frac{\dot{a}}{\alpha}\frac{dh(x)}{dx} \tag{6c}$$

where $\dot{a}/\alpha$ is a dimensionless velocity.

2.4. Elastic field inside craze

The material inside the craze zone, i.e., $y < h(x)$ is modeled by the spring network shown in Fig. 3. The spring network is obtained by periodic extension of the basic unit shown in Fig. 2c. The effective continuum moduli C_{ij} of the resulting spring network are calculated in Ref. [7] and are given in Appendix A. This spring network model simulates the discreteness of the craze microstructure and takes into account of the cross-tie fibrils. The number of spring elements in general depends on the unknown craze thickness $h(x)$. The forces in each element can be computed once $h(x)$ and the traction on the craze-bulk interface is determined.

2.5. Analytical approximations

The problem stated in Sections 2.2–2.4 is fully coupled so that no closed form analytic solution is possible. To gain insight, we propose an approximate analytic solution based on the following simplifying assumptions:

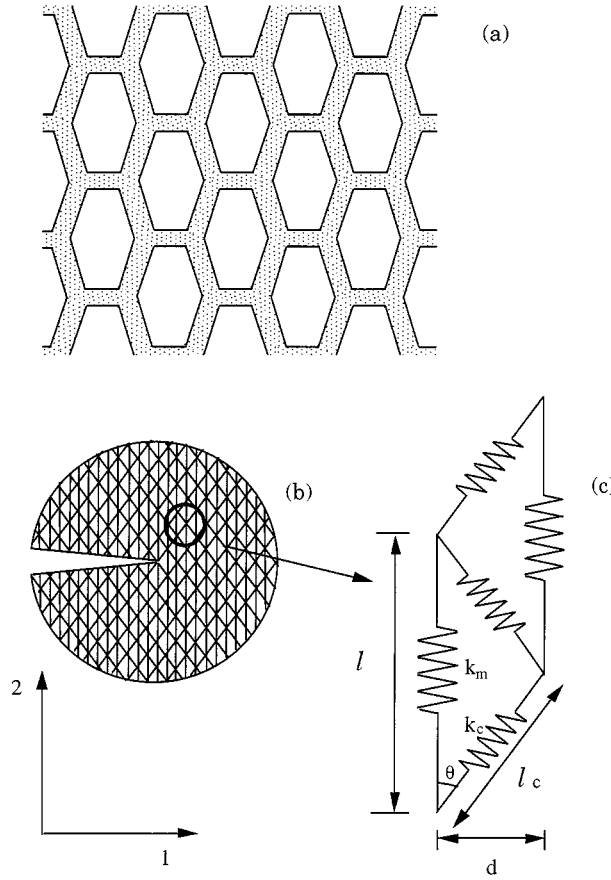

Figure 3 (a) Model of craze microstructure. (b) 2D spring network model used to simulate the craze microstructure. (c) Basic unit of the 2D spring network. The definition of l, l_c, k_m, k_c and d are given in Appendix A.

(1) The normal traction on the unknown craze-bulk interface for $x > 0$ is spatially uniform and is denoted by σ_d. One consequence of this assumption is that the energy release rate G is given by

$$G = 2h_c\sigma_d(1-v_f) \tag{7a}$$

where $2h_c$ is the craze thickness at the crack tip. A detailed discussion of Equation 7a can be found in Ref. [6]. Recall that G is related to the applied stress intensity factor K_A by

$$G = (1-\nu^2)K_A^2/E \tag{7b}$$

(2) The stresses inside the craze is obtained by modeling the craze as a strip with uniform thickness h_c. Unlike the rate independent case, h_c is a function of $\dot{a}$. The spring network model is replaced by an equivalent anisotropic continuum with modulus C_{ij} as described in Appendix A.

The validity and accuracy of the analytical approximate solution is justified by a detailed numerical simulation which is given in Appendix B. In the numerical simulation, the craze material is modeled using the spring network model described in Section 2.4.

Following our assumptions, the stress distribution along the unknown craze-bulk interface $\sigma_n(x)$ is

$$\sigma_n(x) = \sigma_d \quad \text{for } x > 0$$
$$\sigma_n(x) = 0 \quad \text{for } x < 0 \tag{8}$$

Using Equations 6 and 6c, the drawing stress, σ_d, and the applied far field stress intensity factor, K_A, are found to be

$$\sigma_d \left(\frac{\dot{a}}{\alpha}\frac{h_c}{L}\right)^{1/n} \sigma_0 \tag{9a}$$

$$K_A = \frac{2\sqrt{2}}{\sqrt{\pi}}\sigma_d\sqrt{L} \tag{9b}$$

where $2h_c$ is the craze thickness at the crack tip ($x = 0$). Note that h_c and L in Equations 9a and 9b are functions of $\dot{a}$. Integrating Equation 6a and using Equations 5 and 9b, the craze thickness profile is found to be

$$h(\hat{x}) = \frac{(1-\nu^2)K_A^2}{4E(1-v_f)\sigma_d}\left(2\sqrt{1-\hat{x}} + \hat{x}\log\left(\frac{1+\sqrt{1-\hat{x}}}{1-\sqrt{1-\hat{x}}}\right)\right) \tag{10a}$$

where $\hat{x} = x/L$ is the normalized distance. The thickness of the craze at the crack tip, h_c, i.e., $x = 0$ in Equation 10a, is

$$h_c = \frac{(1-\nu^2)K_A^2}{2E(1-v_f)\sigma_d} = \frac{4(1-\nu^2)\sigma_d L}{\pi E(1-v_f)} \tag{10b}$$

Combining Equations 10b with 9a, the drawing stress along the craze-bulk interface, σ_d, is found to be

$$\sigma_d = \left(\frac{4(1-\nu^2)}{\pi E(1-v_f)}\frac{\dot{a}}{\alpha}\sigma_0\right)^{1/(n-1)}\sigma_0 \tag{11}$$

Döll [9] has conducted detailed experimental studies on the craze ahead of a steady state propagating crack inside a homogeneous polymer PMMA. His experimental measurements of the drawing stress versus the steady state crack growth rate is plotted in Fig. 4 [9]. The solid line in Fig. 4 is obtained using our solution for the drawing stress σ_d to fit Döll's data. The fitting parameters are $\alpha = 10^{-4}$ m/s, $\sigma_0 = 100$ MPa and $n = 30$. The experimental data is fitted up to crack growth rate less than 1 m/s. The reason is that at higher velocities, adiabatic heating at the craze-bulk interface will cause the drawing stress to level off (as shown in Fig. 4). This phenomenon cannot be predicted using our simple rate dependent drawing law (Equation 3). In previous studies [5–8], σ_d is assumed to be a material constant independent of the crack growth rate. Note that the expression for σ_d (Equation 11) is independent of the failure criterion.

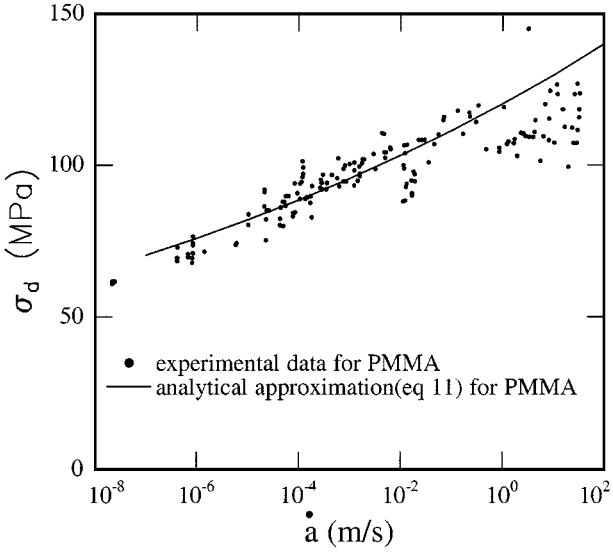

Figure 4 The drawing stress dependence on the crack growth rate for PMMA. The filled circles are from the experimental measurements of Döll [9] and the solid line is the fit of analytical expression (Equation 11) to the experiments.

2.6. Approximate stress field inside the craze

The results in the last section allow us to determine the rate dependent traction σ_d on the craze-bulk interface and the thickness of the craze at the crack tip in terms of K_A and $\dot{a}$. For a given crack growth rate $\dot{a}$, the applied far field stress intensity factor K_A is determined if a failure criterion is specified. To enforce the failure criterion, we need to obtain the stresses on the fibrils directly ahead of the crack tip. Following our assumption 2, these stresses are obtained using the uniform strip model of Brown [5] where the thickness of the strip is given by Equation 10b. When the traction on the craze-bulk interface has the form given by Equation 8, the normal stress ahead of the crack tip inside the craze zone, $\sigma_2(x, y = 0)$ is found to be well approximated by [7]

$$\sigma_2(x, y = 0) = \frac{\sigma_d}{\sqrt{1 - \exp\left(-\frac{\pi x}{h_c\alpha_0}\right)}} \tag{12a}$$

where $\alpha_0^2 = C_{66}/C_{22}$. In particular, the average stress in the first fibril directly ahead of the crack tip, σ_a, is

$$\sigma_a = \sigma_2(x = D, y = 0) = \frac{\sigma_d}{\sqrt{1 - \exp\left(-\frac{\pi D}{h_c\alpha_0}\right)}} \tag{12b}$$

The characteristic distance D is an unknown parameter which is used to match the discrete model, i.e., stress at the first crack tip fibril, to the continuum solution (Equation 12a) and is found to be $d/2$ [7], where d is the fibril spacing.

3. A rate independent fracture criterion

Following Brown [5] we first assume that crack growth occurs when the average stress on the fibril immediately

ahead of the crack tip, σ_a, reaches the breaking stress, σ_f, [5–8]

$$\sigma_a = \sigma_f = \Sigma_{eff} f_b \tag{13a}$$

where f_b is the force required to break a backbone bond of polymer and Σ_{eff} is the number of entangled strands per nominal unit craze area which is given by [7, 18]:

$$\Sigma_{eff} = q\Sigma\left(1 - \frac{M_e}{qM_n}\right) \tag{13b}$$

where Σ is the areal density of entangled strands which cross a plane in the undeformed polymer glass, q is the ratio of the entangled strand density before crazing to that after crazing, M_e is the entanglement molecular weight and M_n is the number average molecular weight of polymer before crazing. Note that this failure criterion corresponds to a rate independent chain scission mechanism.

When the average stress in the first fibril ahead of the crack tip, or more precisely when the tensile stress at $x = d/2$, which is given by Equation 12b, reaches the failure stress, the craze is assumed to fail, i.e.,

$$\frac{\sigma_d}{\sqrt{1 - \exp\left(-\frac{\pi d}{2h_c\alpha_0}\right)}} = \sigma_f = \Sigma_{eff} f_b \tag{14}$$

with σ_d given by Equation 11 and is a function of the crack growth rate.

Paredes and Fischer [19, 20] have found that the product $\sigma_d d$ is a constant, where d is the fibril spacing. Since σ_d is dependent on the crack growth rate, this means that the dimensions of the craze microstructure also depend on the crack velocity. Kramer [1] has shown that

$$\sigma_d d = \frac{8\Gamma}{\beta_0} = A_0 \tag{15}$$

where Γ is the energy to create new surface at craze tip or craze-bulk interface including an energy of primary chain rupture. β_0 is the coefficient of proportionality between average hydrostatic stress and tensile stress, σ_d, at the craze-bulk interface. Equation 15 implies that the fibril spacing and drawing stress are interdependent and throughout this paper, we will assume the product of $\sigma_d d = A_0$ to be a constant.

Equations 14 and 15 allow us to solve for the critical craze thickness at the crack tip, h_c, as a function of the crack velocity $\dot{a}$ and material constants, i.e.,

$$h_c = \frac{-\pi A_0}{2\alpha_0\sigma_d \ln\left[1 - \left(\frac{\sigma_d}{\Sigma_{eff} f_b}\right)^2\right]} \tag{16a}$$

where σ_d is given by Equation 11. The critical crack tip opening displacement, δ_c, is related to h_c by Equation 1.

The relationship of the stress intensity factor K_A and the energy release rate G to $\dot{a}$ can be computed using Equation 7a and 7b

$$K_A^2 = \frac{-\pi(1 - v_f)A_0 E}{\alpha_0(1 - \nu^2)\ln\left[1 - \left(\frac{\sigma_d(\dot{a})}{\Sigma_{eff} f_b}\right)^2\right]} \tag{16b}$$

where $A_0 = 8\Gamma/\beta_0$

$$G = \frac{-\pi(1 - v_f)A_0}{\alpha_0 \ln\left[1 - \left(\frac{\sigma_d(\dot{a})}{\Sigma_{eff} f_b}\right)^2\right]} \tag{16c}$$

Fig. 5a shows the dependence of the craze thickness at the crack tip, h_c, on normalized velocity $\dot{a}/\alpha$ using Equations 16a and 11. We expect that at high crack propagating speed, the craze is thin, since at high speed the craze has less time to thicken. When the crack propagates slowly ($\dot{a}/\alpha$ is small), the craze has enough time to form fully and the craze is thick. This is indeed what Fig. 5a shows. However, we notice that this result (h_c decreases when $\dot{a}/\alpha$ increases) is inconsistent with experimental observations [9, 10] which show the opposite trend (h_c increases when $\dot{a}$ increases).

Fig. 5b shows a plot of G versus $\dot{a}/\alpha$ using Equation 16c. It shows that G decreases monotonically as $\dot{a}/\alpha$ increases. This result is also inconsistent with

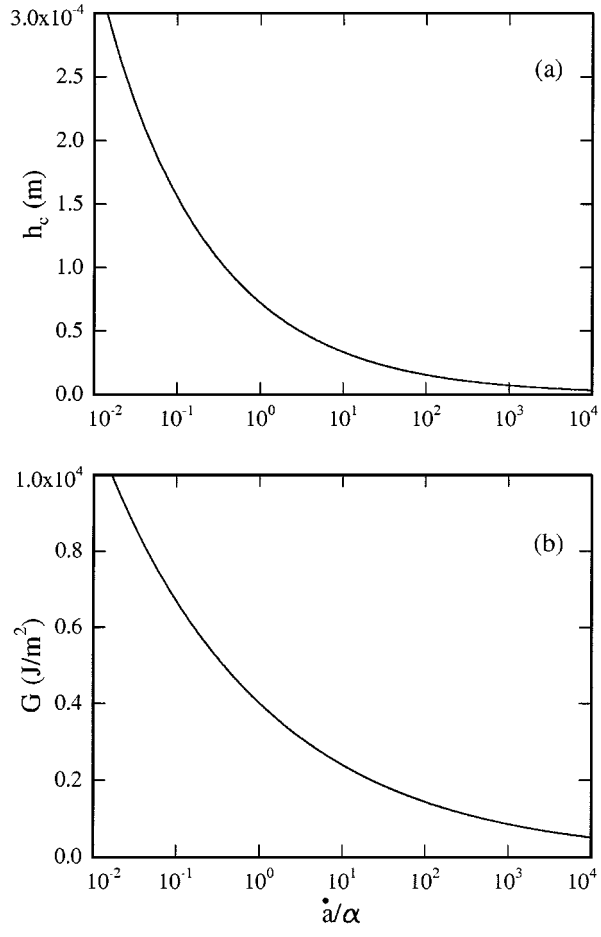

Figure 5 (a) The dependence of h_c on $\dot{a}/\alpha$ using Equation 16a. (b) The dependence of G on $\dot{a}/\alpha$ using Equation 16c.

experimental results, which show that the fracture toughness increases as velocity increases [10]. This discrepancy is due to the rate independent fracture criterion we have used (Equation 13a). Equation 9a implies that the drawing stress σ_d increases as $\dot{a}$ increases (see Fig. 4). If the fibril failure stress σ_f is independent of $\dot{a}$, then the thickness of the craze has to decrease with increasing $\dot{a}$ for otherwise the stress in the crack tip fibril will exceed σ_f according to Equation 14. The experimental observations can therefore only be reconciled by assuming that σ_f increases with $\dot{a}$. Two physically reasonable models for this dependence are described in Section 4 below.

4. Rate dependent failure models

In this section, we re-examine the dependence of the energy release rate G and the craze thickness at the crack tip, h_c, on the crack propagating velocity $\dot{a}$, based on two rate dependent failure criteria: chain scission and chain disentanglement.

4.1. Chain scission

A polymer chain can exist in a bonded state or in a broken state. If the polymer is stable, the energy levels of these two states must be different as shown in Fig. 6. The initial energy difference between the bonded and broken states is $2\Delta G^0$. In order for a polymer chain to break, it must pass over an energy barrier $G^* + \Delta G^0$, and for bond reformation, an energy barrier $G^* - \Delta G^0$. When a normal stress, σ, is applied in the direction of bond breakdown, it causes a reduction of the free energy barrier to break the chain. Analogously, there is an increase in the barrier height for the healing of a broken bond as shown in Fig. 6. Assuming the number of chains in one fibril is N, the rate of breakdown is [13, 21, 22]

$$-\dot{N} = N\frac{\lambda k_B T}{h}\left[\exp\left(-\frac{G^* + \Delta G^0 - \sigma\lambda A/(2N)}{k_B T}\right) - \exp\left(-\frac{G^* - \Delta G^0 + \sigma\lambda A/(2N)}{k_B T}\right)\right] = N\frac{\lambda k_B T}{h}\exp\left(-\frac{G^*}{k_B T}\right)2\sinh \times\left(\frac{\sigma\lambda A/(2N) - \Delta G^0}{k_B T}\right) \quad (17)$$

where λ is the bond displacement between the bonded and broken state as shown in Fig. 6, A is the cross sectional area of the fibril, k_B is the Boltzmann constant, h is the Planck's constant and T is the absolute temperature.

Steady state crack propagation (Equation 4) implies that $\dot{N} = -\dot{a}N_{,x}$, so that Equation 17 becomes

$$\sigma = \frac{2\Delta G^0 N}{\lambda A} + \frac{2Nk_B T}{\lambda A}\sinh^{-1}\left(\dot{a}N_{,x}\frac{h}{2N\lambda k_B T}e^{G^*/k_B T}\right) \quad (18a)$$

Equation 12a implies that the stress decreases rapidly to its nominal value σ_d at very small distance from the crack tip. This allows us to use the simplifying assumption that all the chain scission happens at the first fibril ahead of the crack tip, i.e., $N = \Sigma_{eff}A$, $N_{,x}|_{x=d} \cong N/d$, so the stress needed to fail the first fibril ahead of the crack tip σ_f can be computed from Equation 18a, i.e.,

$$\sigma_f = \frac{2\Delta G^0\Sigma_{eff}}{\lambda} + \frac{2k_B T\Sigma_{eff}}{\lambda}\sinh^{-1}\left(\dot{a}\frac{h}{2\lambda k_B T d}e^{G^*/k_B T}\right) = \sigma_1 + \sigma_2\sinh^{-1}(\dot{a}/\beta) \quad (18b)$$

where

$$\sigma_1 = \frac{2\Delta G^0\Sigma_{eff}}{\lambda} \quad (19a)$$

$$\sigma_2 = \frac{2k_B T\Sigma_{eff}}{\lambda} \quad (19b)$$

$$\beta = \beta_0/\sigma_d \quad \text{and} \quad \beta_0 = \frac{2\lambda k_B T A_0}{h}e^{-G^*/k_B T} \quad (19c)$$

In Equation 18b, σ_1 is the rate independent failure stress for polymer chain and $\sigma_1\sinh^{-1}(\dot{a}/\beta)$ is the contribution due to the rate dependent drawing and failure. For PMMA, ΔG^0 is estimated to be 3.5×10^{-20} J [22] and Σ_{eff} to be 0.285 strands/nm^2 [7, 23]. The separation distance λ is on the order of 1 Å for C−C bond. Using these values, it is found that $\sigma_1 \approx 200$ MPa and $\sigma_2 \approx 25$ MPa for $T = 300$ K. As a check, the force f_b

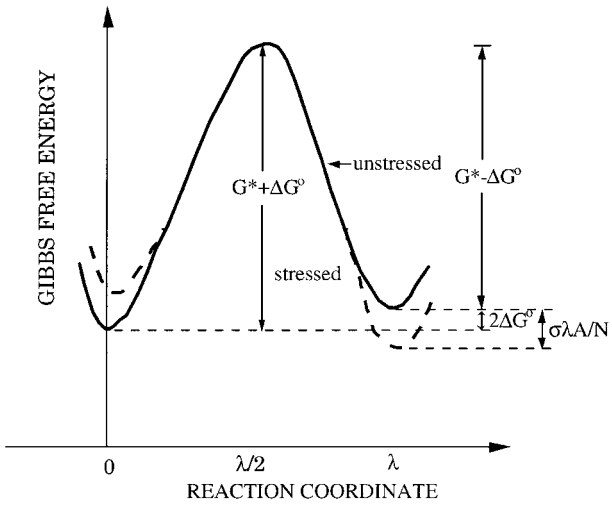

Figure 6 The free energy diagram for the bonded and broken state. The solid line represent the stress free state where there is an initial energy difference $2\Delta G^0$ for the two states. The dashed line represent the free energy curve after a normal stress is applied.

needed to break one polymer chain in the low velocity limit can be found using Equation 18b (with $\sigma_f \approx \sigma_1$) to be 0.7×10^{-9} N, which is consistent with previous estimates [12, 24].

The half thickness of the craze at the crack tip h_c, can be obtained using Equation 14 with σ_f replaced by Equation 18b. This results in

$$h_c = \frac{-\pi A_0}{2\alpha_0 \sigma_d \ln\left[1 - \left(\frac{\sigma_d}{\sigma_1 + \sigma_2 \sinh^{-1}(\dot{a}/\beta)}\right)^2\right]} \quad (20a)$$

The relationship between the stress intensity factor and $\dot{a}$ can be computed using Equation 7b as

$$K_A^2 = \frac{-(1 - v_f)\pi E A_0}{(1 - \nu^2)\alpha_0 \ln\left[1 - \left(\frac{\sigma_d}{\sigma_1 + \sigma_2 \sinh^{-1}(\dot{a}/\beta)}\right)^2\right]} \quad (20b)$$

Note that A_0 in Equations 20 is a material constant given by Equation 15 and that σ_d is a function of $\dot{a}$ (Equation 11).

Fig. 7a shows the dependence of K_A on $\dot{a}$ as predicted by Equation 20a using $\beta = 10$ N/(m s). This choice of β_0 is used to fit the experimental data of Döll [9]. There are two branches in the K_A versus $\dot{a}$ curve. The upper branch corresponds to the higher crack velocity whereas the lower branch gives a lower crack velocity for the same K_A. The lower branch is unstable in the sense that, for a fixed $K > K_A^c$, a slight increase in the crack velocity will cause the stress on the first fibril to increase beyond its critical value, thus causing further acceleration of the crack until the higher velocity is reached on the stable branch. In a load controlled experiment, the upper branch of the K_A versus $\dot{a}$ curve is observed. Note that there exists a critical stress intensity factor K_A^c (at $\dot{a}_c$) below which there is no steady state solution. This also agrees qualitatively with the experimental results [11].

Although there are experimental data on a craze formed ahead of a crack growing at a constant velocity in a homopolymer, very little is known about the failure mechanism of the craze at the fibril level. Assuming that chain scission is the dominant failure mechanism in Döll's experiments, we compare the analytical prediction (Equation 20b) with Döll's experimental data which is shown in Fig. 7b as open circles. The unstable part of the K_A versus $\dot{a}$ curve (in Fig. 7a) is not shown. Although reasonable agreement between our theory and Döll's data is found for $\dot{a} < 1$ m/s, the theoretical curve has a different curvature than the experimental data especially at high velocity. This may be because adiabatic heating at the craze bulk interface at these crack velocities lowers σ_d below the value predicted by Equation 11. This hypothesis is supported by the actual data of Döll for σ_d shown in Fig. 4. To test this hypothesis, we refit Döll's data for $\dot{a} > 1$ m/s using Equation 20b, assuming that σ_d has a constant value of 100 MPa. The analytical fit is shown as stars in Fig. 7b. The resulting fit is improved somewhat but it is clear that our analytical results still underestimate K_A at larger velocities. Note that heating at the craze-bulk interface will cause other changes besides just decreasing the drawing stress. For example, it increases the likelihood of disentanglement during the fibrillation process, so that q, the ratio of the entangled strand density before crazing to that after crazing, increases at sufficiently high velocities. Since the force needed to break a fibril is proportional to q, an increase in q will lead to further increase in K_A. This effect is not included in out model (Equation 20b) which assumes q to be a constant.

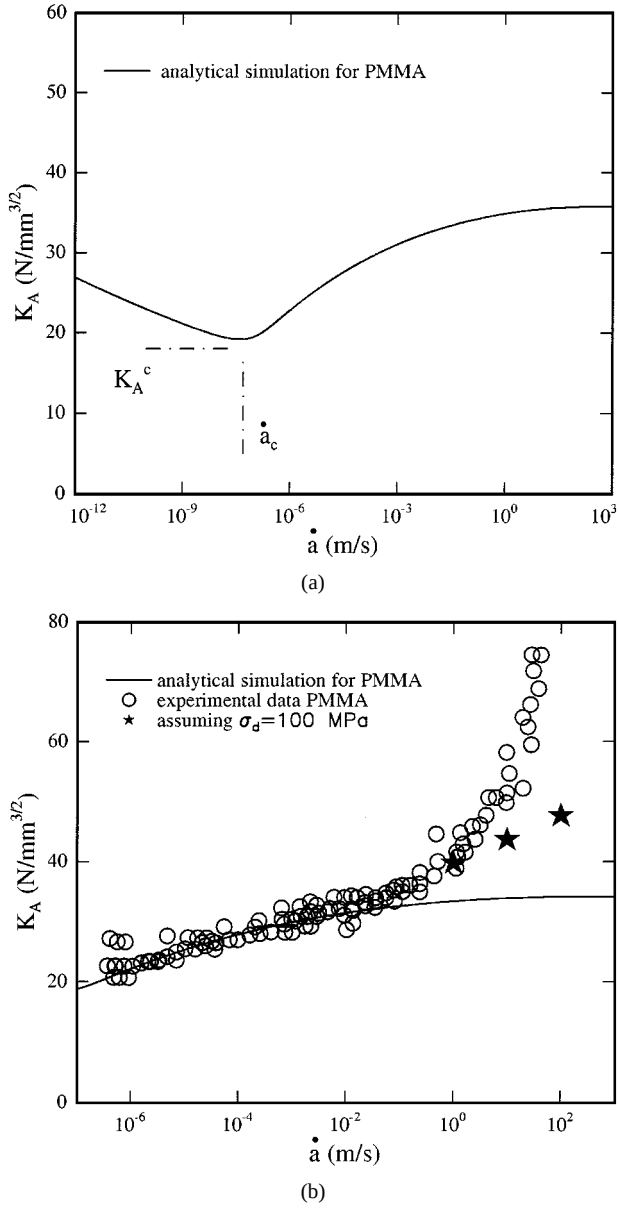

Figure 7 (a) Plot of applied stress intensity factor K_A versus the crack propagation velocity $\dot{a}$ (Equation 20b) for PMMA. (b) The solid line is the analytical solutions based on the rate dependent chain scission craze failure criterion while the open circle is the experimental data from Döll.

4.2. Chain disentanglement

Kramer and Berger [18] have proposed a disentanglement model for a chain in the highly stretched region of the craze fibril near the craze-bulk interface. Here, we modify Kramer and Berger's analysis to consider disentanglement in the fibrils ahead of the crack tip so

that we can study the process of craze fibril breakdown by disentanglement.

Consider a molecule in a drawn fibril consisting of a number of extended molecular lengths between entanglements. The length of these is taken to be the contour length between entanglement $l_e = l_0(M_e/M_0)$, where l_0 is the projected length of the mer along the chain and M_e and M_0 are the entanglement molecular weight and the mer molecular weight, respectively. The monomer frictional force in a direction away from the center of the chain, f_m, is assumed to be a nonlinear function of the velocity of a monomer along the chain relative to its surroundings v_m, i.e.,

$$\begin{aligned} (f_m)^p &= v_m\zeta_0 \qquad \text{for } v_m > 0 \\ (-f_m)^p &= -v_m\zeta_0 \quad \text{for } v_m < 0 \end{aligned} \tag{21}$$

where ζ_0 is the monomer friction coefficient and $p > 0$ is a material constant. In Kramer and Berger's original work, a linear relation is assumed between f_m and v_m, i.e., $p = 1$.

Following Kramer and Berger's analysis, the normal stress σ on a fibril is found to satisfy

$$\left(\frac{\sigma}{\sigma_e}\right)^p = \dot{\delta} \tag{22a}$$

where $\dot{\delta}$ is the rate of disentanglement and δ is the contour length between entanglements. σ_e is a material constant and its expression in terms of molecular parameter is

$$\begin{aligned} \sigma_e = {} & \frac{M_e}{M_0 d^2}(\zeta_0)^{1/p}\frac{2p}{p+1} \\ & \times\left[\frac{4M_e}{M_n'}\frac{p}{2p+1}\left[1-\left(1+\frac{M_n'}{4M_e}\right)^{(2p+1)/p}\right]\right. \\ & \left.+\left(1+\frac{M_n'}{4M_e}\right)^{(p+1)/p}\right] \end{aligned} \tag{22b}$$

where d is the fibril spacing. The derivation of Equations 22a and 22b is given in Appendix C. M_n' in Equation 22b is the number average molecular weight of the polymer fibrils. M_n' differs from M_n, the number average molecular weight of the bulk polymer, since chains are broken during fibril formation by surface drawing. Its relation to M_n is [1]

$$\frac{1}{M_n'} = \frac{1}{M_n} + \frac{1-q}{M_e}$$

where q is the ratio of the entangled strand density before crazing to that after the crazing.

The amount of disentanglement in the fibril at a distance x ahead of the crack tip is obtained by integrating Equation 22a subjected to the steady state condition (Equation 4), i.e.,

$$\dot{\delta} = -\dot{a}\frac{\partial\delta}{\partial x}$$

According to Equation 22a, the amount of disentanglement at x is

$$\left(\frac{\sigma(x)}{\sigma_e}\right)^p = -\dot{a}\frac{\partial\delta(x)}{\partial x} \tag{22c}$$

For the disentanglement failure mechanism, the craze will fail when the network strands in the first fibril ahead of the crack tip ($x = d$) are totally disentangled, i.e., $\delta(d) = \delta_0$ where δ_0 is the critical value for a fibril to disentangle fully and is found to be [1, 18]

$$\delta_0 = l_e(1 + M_n'/2M_e)$$

At the craze tip, $x = L$, the craze fibrils are assumed to be fully entangled, that is $\delta(L) = 0$. Using Equation 22c and $\delta(L) = 0$, we have

$$\delta(x) = \int_L^x \frac{\partial\delta}{\partial s}\mathrm{d}s = \int_L^x -\frac{1}{\dot{a}}\left(\frac{\sigma(s)}{\sigma_e}\right)^p \mathrm{d}s \quad 0 < x < L \tag{23}$$

Integrating Equation 23 and enforcing the failure criterion $\delta(d) = \delta_0$, we obtain

$$L \cong \delta_0\dot{a}\left(\frac{\sigma_d}{\sigma_e}\right)^{-p} \tag{24}$$

where σ_d and σ_e are given by Equations 11 and 22b, respectively. The derivation of Equation 24 is given in Appendix D.

Substituting Equation 24 into Equation 10b, the following explicit expressions for h_c and K_A are obtained,

$$h_c = \frac{4(1-\nu^2)\delta_0}{(1-\nu_f)\pi E}\sigma_d^{1-p}\sigma_e^p\dot{a} \tag{25a}$$

$$K_A = \frac{2\sqrt{2\delta_0\dot{a}}}{\sqrt{\pi}}\sigma_d^{1-p/2}\sigma_e^{p/2} \tag{25b}$$

where σ_d is a function of velocity and is given by Equation 11.

Using Equations 7a and 25a, the energy release rate is related to $\dot{a}$ by,

$$G = A_1(\dot{a})^{(n+1-p)/(n-1)} \tag{26}$$

where

$$A_1 = \frac{8(1-\nu^2)\delta_0}{\pi E}\left(\frac{4(1-\nu^2)\sigma_0}{\pi E(1-\nu_f)}\right)^{(2-p)/(n-1)}\sigma_0^{(2-p)}\sigma_e^p.$$

Recent experiments of strengthening a polymer/polymer bi-material interface using a deuterated polystyrene-polyvinylpyridine (dPS-PVP) diblock copolymer with a moderately long dPS block (540 units), showed that the dominant craze failure mechanism is disentanglement [11]. The results obtained above can be used to estimate the craze failure at such interfaces, e.g., a PS/PVP interface reinforced using dPS-PVP block copolymers. Experiments have shown that a craze can only form at the PS side of the PS/PVP interface [26]. Assuming the displacement of the PVP

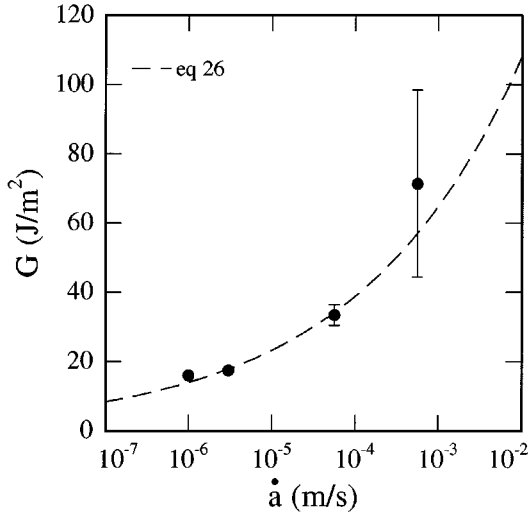

Figure 8 Plot of energy release rate G versus the crack propagation rate $\dot{a}$. The solid line are the plot of the analytical solution using the rate dependent chain disentanglement craze failure criterion (Equation 26). The filled circles are the experimental measurement for a PS/PVP interface [10] reinforced by 540–510 dPS-PVP diblock copolymer at a grafting density of $\Sigma = 0.14$ chains/nm^2. The error bar on the experimental results represents the standard deviation.

surface is negligible compared with the stretch of the craze microstructure, the craze formed at the bimaterial interface is similar to the half craze we have studied in this paper. This is because in our simulation, we only consider the upper half plane ($y > 0$) due to symmetry. Since the craze cannot form on the PVP side, the G for the bimaterial interface is equal to $G/2$ in this paper. Therefore we can use the same analytical expressions, e.g., Equation 26 for disentanglement, to study craze breakdown at a bi-material interface, e.g., PS/PVP. Fig. 8 plots the interface fracture toughness G versus $\dot{a}$ for a PS/PVP interface reinforced with a dPS-PVP diblock polymer [10]. The solid line represents Equation 26 of the disentanglement model (Section 4.2), where we have chosen $A_1 = 300$ and $p = 9$, and we have assumed that $n = 10$ for PS. Reasonable agreement is found between the simulation (Equation 26) and the experimental results.

5. Conclusion

We have extended the strip model of Brown to predict the rate dependent stresses inside the craze. For the power law drawing model used in this study, the strip model provides an approximate analytical solution for the crack tip stresses as demonstrated by our numerical simulation. We anticipate that this can be extended to include different drawing laws, thus avoiding the difficult problem of finding numerical solution to the coupled rate dependent boundary value problem.

In the rate independent limit, the fracture of the polymer glass can be characterized by either a critical energy release rate G_c or a critical stress intensity factor K_c. This is no longer possible when the material behavior is rate dependent. In general, the crack growth rate is controlled by the entire stress history ahead of the crack tip. For the special case of steady state, we have found relations between $\dot{a}$ and $K_A(G)$. The exact relations depend on the failure mechanism of the fibrils ahead of the crack tip.

We have demonstrated that a rate independent craze failure criterion cannot explain the experimental observations of craze fracture even if rate dependent drawing of the craze fibrils is taken into consideration. Rate dependent craze failure criteria have to be used to obtain relations between K_A and the crack growth rate $\dot{a}$ that are consistent with experimental results. The dependence of the drawing stress σ_d and the craze thickness at the crack tip h_c on $\dot{a}$ has been explicitly derived, using rate dependent chain scission and disentanglement models.

Appendix A: Characteristics of the spring network

The spring network used in the calculation is formed by translation of a unit cell as shown in Fig. 3. The springs which model the main fibrils have spring constant k_m whereas the cross-tie fibrils have spring constant k_c. The distance between the main fibrils is denoted by d and the angle between the cross-tie fibrils and main fibrils is denoted by θ. The cross-section areas (and lengths) of the main fibrils and the cross-tie fibrils are denoted by A_m and A_c (l and l_c) respectively.

For the stress-strain relation shown below:

$$\begin{aligned} \sigma_{11} &= C_{11}\varepsilon_{11} + C_{12}\varepsilon_{22} \\ \sigma_{22} &= C_{12}\varepsilon_{11} + C_{22}\varepsilon_{22} \\ \sigma_{12} &= 2C_{66}\varepsilon_{12} \end{aligned} \tag{A1}$$

where the constants C_{ij} are defined by:

$$\begin{aligned} C_{11} &= E_c \sin^4\theta \quad C_{12} = E_c \sin^2\theta \cos^2\theta \\ C_{22} &= E_m + E_c \cos^4\theta \quad C_{66} = C_{12} \end{aligned} \tag{A2}$$

E_m (E_c) is the effective modulus of the main (cross-tie) fibrils and is defined by:

$$\begin{aligned} E_m &= v_m E_m = v_m k_m l / A_m \\ E_c &= v_c E_c = v_c k_c l_c / A_c \end{aligned} \tag{A3}$$

where l and l_c denote the length of main and cross-tie fibrils respectively. In Equation A3, $E_m = k_m l / A_m$ is the extension modulus of a typical main fibril and $E_c = k_c l_c / A_c$ is the extension modulus of a typical cross-tie fibril. Let V_m and V_c denote the volumes occupied by the main and cross-tie fibrils in a unit cell, then $v_m = V_m / V_{cell}$, $v_c = V_c / V_{cell}$ are the volume fractions of the main fibrils and the cross-tie fibrils respectively.

Appendix B: Justification of the approximate analytical solution using full-field numerical simulation

To check the validity and accuracy of the analytical solution presented above, a full field numerical simulation is conducted. As in Ref. [8, 27], we decompose the problem into two parts. Part I is the solution of the exterior elastic problem (bulk polymer) with

unknown traction $-\sigma_n(x)$ acting on the surface of a semi-infinite crack loaded under small scale yielding conditions [14–16]. Problem II is the solution of the interior problem (craze) with $\sigma_n(x)$ acting on the unknown craze surface defined by $h(x)$.

For the interior problem, the craze microstructure is modeled using a 2D discrete spring network model as described in Appendix A. For the plane strain analysis, the fibrils are treated as sheets with stiffness equivalent to layers of fibrils spaced at distance d. Out-of-plane cross-tie fibrils are neglected. This approximation has been examined using a 3D network of springs and has been found to adequately represent the 3D situation [27]. The numerical values for the 2D spring network, and a detailed discussion of how its parameters were obtained, are given in reference [7, 8].

Details of the numerical implementation of the outer and inner problem based on the rate dependent drawing law (Equation 3) and the rate independent failure criterion (Equation 13a) can be found in reference [7, 27]. The numerical simulation are based on parameters for polystyrene (PS). The normalized normal stress $\sigma_n(x)/\sigma_0$ distribution on the craze-bulk interface for different normalized non-dimensional craze velocities ($\dot{a}/\alpha$) is shown in Fig. 9. The x axes is normalized with respect to the craze length L. Fig. 9 shows that the faster the crack propagates, the higher is the normal traction on the craze-bulk interface. Note that for the highest crack velocity, $\dot{a}/\alpha = 400$ in our simulation, the normal stress along the craze-bulk interface exhibits a stress concentration near the crack tip. For slower crack velocities, i.e., $\dot{a}/\alpha = 3$, the stress on the craze-bulk interface is low and is practically uniformly distributed along the craze-bulk interface. Fig. 9 also shows that the Dugdale model is a good approximation for the stress distribution along the craze-bulk interface. Note that the results near the craze tip ($x = L$) are not shown in Fig. 9. This is because in the numerical solution of the non-linear integral equation of Equation 6a, substantial error is introduced near $x = L$ [28, 29]. However, it was shown in Ref. [28] that the error is localized at $x = L$ and thus does not affect the stress near thecrack tip.

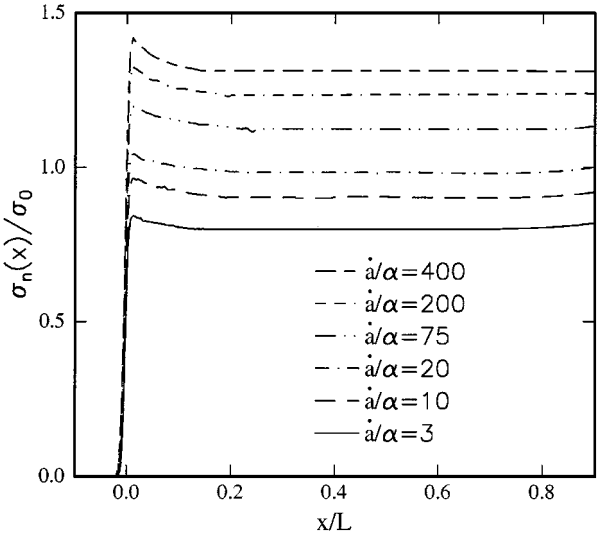

Figure 9 The normalized normal stress $\sigma_n(x)/\sigma_0$ distribution on the craze-bulk interface for different crack growth rates.

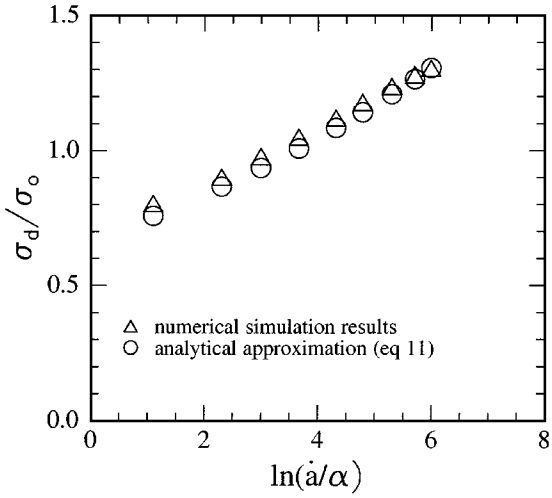

Figure 10 The plot σ_d/σ_0 versus $\ln(\dot{a}/\alpha)$. The numerical simulation results are plotted as triangles. The approximate analytical solutions of Equation 11 are plotted as open circles.

The σ_d/σ_0 dependence on $\ln(\dot{a}/\alpha)$ given by our numerical simulations is shown as triangles in Fig. 10, where σ_d, based on our numerical simulation results, is calculated by taking the averages of $\sigma_n(x)$ far away from the crack tip and away from the craze tip, i.e., $0.1L < x < 0.9L$. The corresponding analytical expression (Equation 11) is plotted as open circles in Fig. 10. Good agreement is obtained between the numerical simulation results and the analytical approximation (Equation 11).

Fig. 11a shows the dependence of the normalized craze thickness at the crack tip h_c/d on $\ln(\dot{a}/\alpha)$. The simulation results are plotted as triangles. The analytical expression of Equation 16a, with σ_d given by Equation 11, is plotted as open circles in Fig. 11a. Good agreement is obtained between the numerical results and the analytical expressions (Equation 16a). Fig. 11b shows a plot of $K_A/(\sigma_0\sqrt{d})$ versus $\ln(\dot{a}/\alpha)$. The numerical simulation results are shown as triangles in Fig. 11b whereas the analytical expression of Equation 16b is plotted as open circles. Good agreement is obtained for thick crazes (low $\dot{a}/\alpha$ corresponds to a thick craze).

Appendix C: Derivation of Equation 22

Following Kramer and Berger [18], v_m can be approximated by

$$v_m = \Delta v\left[1 - \frac{M_n'}{2M_e}\left(x' - \frac{1}{2}\right)\right] \quad x' < \frac{1}{2}$$
$$v_m = \Delta v\left[-1 - \frac{M_n'}{2M_e}\left(x' - \frac{1}{2}\right)\right] \quad x' > \frac{1}{2} \tag{C1}$$

where $\Delta v = \dot{\delta}$ is the rate of disentanglement. x' is the fractional distance along the molecule from one of its ends. The force in the chain is given by

$$f(x') = \int \frac{M_n'}{M_0} f_m(\eta)\, d\eta \tag{C2}$$

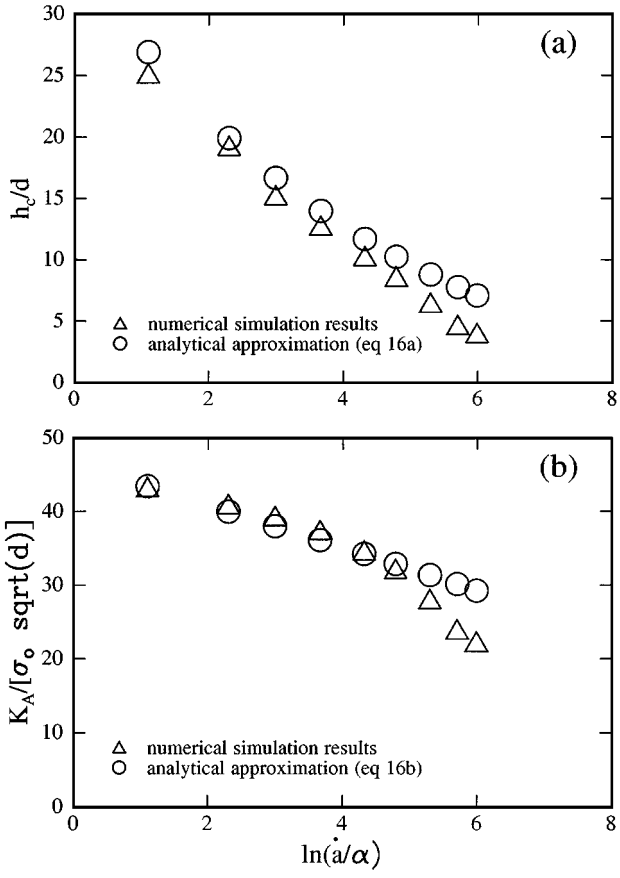

Figure 11 (a) The plot of h_c/d versus $\ln(\dot{a}/\alpha)$. The numerical simulation results are plotted as triangles. The approximate analytical solutions of Equation 16a are plotted as open circles. (b) The plot of $K_A/(\sigma_0\sqrt{d})$ versus $\ln(\dot{a}/\alpha)$. The numerical simulation results are plotted as triangles. The approximate analytical solutions of Equation 16b are plotted as open circles.

with the boundary conditions that the forces are zero at the ends, i.e., $f(0)=0$, $f(1)=0$. Putting Equations 21 and C1 into Equation C2 and for simplicity, only considering p to be an odd number, we have

$$f(x') = \frac{-2M_e}{M_0}(\zeta_0\Delta v)^{1/p}\frac{p}{p+1} \times\left[\left(1-\frac{M_n'}{2M_e}x'+\frac{M_n'}{4M_e}\right)^{(p+1)/p} - \left(1+\frac{M_n'}{4M_e}\right)^{(p+1)/p}\right] \quad x' < \frac{1}{2}$$

$$f(x') = \frac{-2M_e}{M_0}(\zeta_0\Delta v)^{1/p}\frac{p}{p+1} \times\left[\left(-1-\frac{M_n'}{2M_e}x'+\frac{M_n'}{4M_e}\right)^{(p+1)/p} - \left(1+\frac{M_n'}{4M_e}\right)^{(p+1)/p}\right] \quad x' > \frac{1}{2} \quad \text{(C3)}$$

where M_0 is the molecular weight of mer repeat unit and M_e is the entanglement molecular weight.

The average force in the chain $\langle f\rangle$ is given by

$$\langle f\rangle = \int_0^1 f(x')\,dx' = \frac{M_e}{M_0}(\zeta_0\Delta v)^{1/p}\frac{2p}{p+1} \times\left[\frac{4M_e}{M_n'}\frac{p}{2p+1}\left[1-\left(1+\frac{M_n'}{4M_e}\right)^{(2p+1)/p}\right] + \left(1+\frac{M_n'}{4M_e}\right)^{(p+1)/p}\right] \quad \text{(C4)}$$

The normal stress in the fibril is given by $\sigma = \langle f\rangle/d^2$ and the rate of disentanglement is $\dot{\delta} = \Delta v$. Thus Equation C4 can be written as

$$\left(\frac{\sigma}{\sigma_e}\right)^p = \dot{\delta} \quad \text{(C5)}$$

and

$$\sigma_e = \frac{M_e}{M_0 d^2}(\zeta_0)^{1/p}\frac{2p}{p+1} \times\left[\frac{4M_e}{M_n'}\frac{p}{2p+1}\left[1-\left(1+\frac{M_n'}{4M_e}\right)^{(2p+1)/p}\right] + \left(1+\frac{M_n'}{4M_e}\right)^{(p+1)/p}\right]$$

which is Equation 22b.

Appendix D: Derivation of Equation 24

Integrating Equation 23 from L to d using the boundary conditions $\delta(L)=0$ and $\delta(d)=\delta_0$,

$$\int_d^L \left(\frac{\sigma(x)}{\sigma_e}\right)^p dx = \delta_c\dot{a} \quad \text{(D1)}$$

Substituting $\sigma(x)$ in Equation 12a into Equation D1, we obtain

$$\int_d^L \left(\frac{\sigma_d}{\sigma_e}\right)^p \frac{dx}{\left(1-\exp\left(-\frac{\pi x}{h_c\alpha_o}\right)\right)^{p/2}} = \delta_c\dot{a} \quad \text{(D2)}$$

With the change of variable $t=\sqrt{1-\exp(-\pi x/h_c\alpha_o)}$, Equation D2 becomes

$$I_0 = \int_{d_1}^{d_2}\frac{dt}{t^{p-1}(1-t^2)} = \frac{\delta_c\pi}{2h_c\alpha_0}\left(\frac{\sigma_d}{\sigma_e}\right)^{-p}\dot{a} \quad \text{(D3)}$$

where

$$d_1 = \sqrt{1-\exp(-\pi d/h_c\alpha_0)},$$

$$d_2 = \sqrt{1-\exp(-\pi L/h_c\alpha_0)}.$$

I_0 can be integrated exactly for any positive integer p. For an integer p, I_0 is

$$I_0 = \begin{cases} \displaystyle\sum_{i=1}^{k} \frac{-1}{2i-1} t^{-(2i-1)} \Big|_{d_1}^{d_2} \\ \quad + \frac{1}{2}\ln\left(\frac{(1+d_2)(1-d_1)}{1+d_1}\right) - \frac{1}{2}\ln(1-d_2) \\ \qquad \text{for } p = 2k+1, \quad k = 0, 1, \ldots \\ \displaystyle\sum_{i=2}^{k} \frac{-1}{2i-2} t^{-(2i-2)} \Big|_{d_1}^{d_2} \\ \quad + \frac{1}{2}\ln\left(\frac{d_2(1+d_1)(1-d_1)}{d_1(1+d_2)}\right) - \frac{1}{2}\ln(1-d_2) \\ \qquad \text{for } p = 2k, \quad k = 1, 2, \ldots \end{cases} \tag{D4}$$

In our simulation, $d = 17.32$ nm, $\alpha_0 = \sqrt{0.02}$. For a thick craze $h_c = 2\mu$m, d_1 is calculated to be 0.57. Thus in Equation D4, both the first and second term on the right hand side are of order 1 (bounded). Since the length to thickness ratio L/h is large, e.g., $L/h > 10$, $(\pi L/h_c\alpha_0) > 224$ thus $d_2 \approx 1$. Since the other terms in Equation D4 are bounded, the value of I_0 will be dominated by the last term of Equation D4, i.e., $-\frac{1}{2}\ln(1-d_2)$. Using a Taylor expansion and omitting the higher order terms,

$$d_2 = 1 - \frac{1}{2}\exp\left(-\frac{\pi L}{h_c\alpha_0}\right) \tag{D5}$$

The last term of Equation D4 is therefore will be approximated by $(\pi L/2h_c\alpha_o) \gg 1$. We use this as an approximation for I_0 so that Equation D3 becomes $L = \delta_c\dot{a}(\sigma_d/\sigma_e)^{-p}$ which is Equation 24.

From Equation D4, we find that the singular stress distribution near the crack tip $(1 - \exp(-\pi x/h_c\alpha_o))^{-1/2}$ do not substantially affect the disentanglement. Note that in Equation D4,

$$t = \sqrt{1 - \exp(-\pi x/h_c\alpha_o)}.$$

This is because the region of dominance of the singular field as $x \to 0$ is very small for small α_0. The disentanglement failure mechanism of the first fibril ahead of the crack tip is a result of the accumulation of disentanglement along the craze length, L.

Acknowledgements

Y. Sha, C. Y. Hui and E. J. Kramer are supported by the Materials Science Center at Cornell, which is funded by the National Science Foundation (DMR-MRSEC program). The authors would like to thank Professor A. Ruina for valuable discussions.

References

1. E. J. KRAMER, *Adv. Polymer Sci.* **52/53** (1983) 1.
2. A. S. ARGON and M. M. SALAMA, *Mater. Sci. Eng.* **23** (1977) 219.
3. D. S. DUGDALE, *J. Mech. Phys. Solid* **8** (1960) 100.
4. P. BEHAN, M. BEVIS and D. HULL, *Proc. Soc. Lond. A* **343** (1975) 525.
5. H. R. BROWN, *Macromolecules* **24** (1991) 2752.
6. C. Y. HUI, A. RUINA, C. CRETON and E. J. KRAMER, *ibid.* **25** (1992) 3948.
7. Y. SHA, C. Y. HUI, A. RUINA and E. J. KRAMER, *ibid.* **28** (1995) 2450.
8. *Idem., Acta Mater.* **45** (1997) 3555.
9. W. DÖLL, *Adv. Polym. Sci.* **52/53** (1983) 105.
10. C. A. DAI, P. A. SMITH, L. J. NORTON, A. HUBENKO, E. J. KRAMER and C. Y. HUI, to be published.
11. E. J. KRAMER and E. W. HART, *Polymer* **25** (1984) 1667.
12. W. G. KNAUSS and G. U. LOSI, *J. Appl. Mechanics* **60** (1993) 793.
13. Polymer Fracture, edited by H. H. Kausch, 2nd ed. (Springer-Verlag, New York, 1987).
14. C. Y. HUI and A. RUINA, *International Journal of Fracture* **72** (1995) 97.
15. J. R. RICE, in "Fracture," Vol. 2, edited by H. Liebowitz (Academic Press, New York, 1968) p. 191.
16. M. L. WILLIAMS, *J. Appl. Mechanics* **24** (1957).
17. H. TADA, P. PARIS and G. IRWIN, "The Stress Analysis of Cracks Handbook" (Paris Productions, 1985).
18. E. J. KRAMER and L. L. BERGER, *Adv. Polym. Sci.* (1991) 1.
19. E. PAREDES and E. W. FISCHER, *Makromol. Chem.* **180** (1979) 2707.
20. *Idem., J. Polymer Sci.-Polymer Phys.* **20** (1982) 929.
21. A. TOBOLSKY, R. E. POWELL and H. EYRING, in "The Chemistry of Large Molecules," edited by R. E. Burk and O. Grummitt (Interscience Publishers, New York, 1943) p. 125.
22. D. J. MATZ and S. L. COOPER, *Soc. Plast. Eng., Tech. Pap.* **18** (1972) 431.
23. L. L. BERGER, *Macromolecules* **23** (1990) 2926.
24. C. CRETON, E. J. KRAMER, C. Y. HUI and H. R. BROWN, *Macromolecules* **25** (1992) 3075.
25. Polymer Handbook, edited by J. Brandrup and E. H. Immergut, Vol. 77, 3rd ed. (A Wiley-Interscience, New York, 1989).
26. J. WASHIYAMA, C. CRETON and E. J. KRAMER, *Macromolecules* **25** (1992) 4751.
27. SHA, Y., PhD Thesis, Cornell University, Ithaca, NY, 1997).
28. L. O. FAGER and J. L. BASSANI, *J. Eng. Mater. Technol.* **115** (1993) 252.
29. L. O. FAGER, J. L. BASSANI, C. Y. HUI and D. B. XU, *Int. J. Frac.* **52** (1991) 119.

Received 23 February 1998
and accepted 22 January 1999